pss-Header will be provided by the publisher



# Exciton transition and electronic structure of $PbMoO_4$ crystals studied by polarized light

**Masami Fujita [*,1], Minoru Itoh [**,2], Hiroyuki Mitani [2], Sangeeta [3], and Mohit Tyagi [3]**

[1] Japan Coast Guard Academy, Wakaba, Kure 737-8512, Japan
[2] Department of Electrical and Electronic Engineering, Shinshu University, Nagano 380-8553, Japan
[3] Crystal Technology, TPPED, Bhabha Atomic Research Center, Trombay, Munbai 400 085, India

Received ZZZ, revised ZZZ, accepted ZZZ
Published online ZZZ (Dates will be provided by the publisher.)

**PACS** 71.35.Cc, 78.20.Ci, 71.20.-b, 71.20.Ps

* Corresponding author: e-mail fujita@jcga.ac.jp, Phone: +81 823 21 4961, Fax: +81 823 21 8105
** e-mail itohlab@shinshu-u.ac.jp, Phone: +81 26 269 5261, Fax: +81 26 269 5220

Polarized reflectivity spectra of $PbMoO_4$ crystals have been measured using synchrotron radiation up to 20 eV. The optical constants for the crystallographic axes are derived by using a Kramers-Kronig analysis. It is found that the exciton band at 3.6 eV shows a doublet structure with distinct dichroism. X-ray photoemission spectroscopy (XPS) and the calculation of the electronic structure by a discrete variational *Xα* method are also carried out. The calculation shows that the valence band and the conduction band are mainly composed of the O 2p and Mo 4d states, respectively, and the Pb state contributes appreciably to the top of the valence band and the bottom of the conduction band. The valence-band XPS spectrum of $PbMoO_4$ is compared with that of $PbWO_4$, which reveals a remarkable difference between them. This difference reflects different magnitude of hybridization of Mo 4d or W 5d state to the valence band. The exciton transition is explained in terms of the cationic Pb 6s → 6p excitation model taking into account the crystal-field splitting and the spin-orbit interaction of Pb 6p state. From a comparison of the doublet structure of the exciton band of $PbMoO_4$ and $PbWO_4$, it is suggested that the electron-hole exchange interaction plays an important role for the exciton transitions in both materials.



**1 Introduction** Metal tungstates and molybdates are well known as intrinsic scintillating materials [1–4]. Their luminescence properties have been extensively studied [5–9]. The electronic structures of these materials have been calculated theoretically using LAPW method [10, 11], and discrete variational *Xα* (DV-*Xα*) method [12]. A systematic x-ray photoemission spectroscopy (XPS) has been carried out recently on some tungstates [12].

Most of metal molybdates and tungstates crystallize to the scheelite or wolframite structure [13–16]. The scheelite structure is found in the materials with large metal ions such as Pb, Ca, and Ba. On the other hand, the wolframite structure is found in the materials with small metal ions such as Zn, Mn, or Fe. The Cd compounds are on the border; $CdMoO_4$ is of scheelite type and $CdWO_4$ is of wolframite type. We have performed a series of studies on the optical properties of metal tungstates and molybdates [17–21]. From the analyses of the remarkable dichroism found near the absorption edge, we could obtain fruitful information on the electronic structures of these anisotropic crystals. For $PbWO_4$, the sharp absorption band peaking at 4.3 eV is assigned to the exciton transition from the Pb 6s state hybridized with the O 2p valence band to the Pb 6p state hybridized with the W 5d conduction band [18]. The lowest absorption band of Ca compounds is ascribed to the transition from the valence band of O 2p state to the conduction band of Mo 4d (W 5d) state, without clear excitonic structures [19]. In the case of Cd compounds, the structures at the absorption edge are attributed to the transitions from the O 2p valence band to the conduction band which is formed by the strongly hybridized Mo 4d–Cd 5s (W 5d–Cd 5s) states [21]. These experimental results are in good agreement with the results of the DV-*Xα* calculation and the XPS experiment [12, 21].

Information on the exciton states in tungstates and molybdates is deeply desired to understand the de-excitation processes after high-energy electronic excitation, since these materials are widely used for scintillation detectors. In the optical studies mentioned above, we revealed that no structures suggestive of exciton transition are found in $CaMoO_4$, $CaWO_4$, and $CdMoO_4$, while weak exciton bands are observed in $CdWO_4$ and $ZnWO_4$ [19–21]. In contrast to these materials, $PbWO_4$ exhibits a pronounced exciton band with distinct dichroism [18]. We proposed that the anisotropic fine structure of the exciton band in $PbWO_4$ is explained in terms of the cationic Pb 6s → 6p excitation under uniaxial crystal-field along the *c*-axis. Similar cationic exciton transition is expected to take place in $PbMoO_4$. In order to confirm the cationic exciton model and to get more detailed information on the exciton states, it would be interesting to compare the optical spectra of $PbWO_4$ and $PbMoO_4$ crystals, both having the scheelite structure. The optical spectra of $PbMoO_4$ have not been established as yet, although reflection measurements have been reported by a few groups [22, 23].

The $PbMoO_4$ crystals are tetragonal and therefore optically uniaxial. The optical axis is parallel to the crystallographic *c*-axis, while the *a*- and *b*-axes are equivalent to each other. In the present study, reflectivity spectra of oriented $PbMoO_4$ crystals are measured by using polarized synchrotron radiation. Optical constants are calculated with the help of a Kramers-Kronig analysis. The XPS spectrum is also measured to get information on the valence band and core states. The electronic structure of $PbMoO_4$ is calculated using the DV-*Xα* method. The electronic structure and the exciton state are discussed based on the present results of $PbMoO_4$ and the previous studies of $PbWO_4$.

**2 Experiment** $PbMoO_4$ crystals used in the present study were provided from Bhabha Atomic Research Center (BARC) in India and also purchased from Furukawa Company in Japan. Both the crystals were grown by Czochralski technique under normal atmosphere. Details of the crystal growth of BARC samples are described in ref. [24]. The samples of 10×10×2 $mm^3$ were obtained from the crystals oriented by the x-ray diffraction or by means of a pair of crossed polarizers. The surfaces containing *a*- and *c*-axes were polished mechanically for the measurement of reflection. BARC samples were yellowish in color as compared to those from Furukawa, which were nearly colorless. This coloration, however, did not affect the reflectivity spectra.

Optical experiments were carried out using a 1m Seya-Namioka type monochromator at the beamline 1B in UVSOR facility of the Institute for Molecular Science in Okazaki. The samples were mounted on the copper holder in a variable temperature cryostat of He-flow type. The base pressure of the sample chamber was kept at about $1.0\times10^{-6}$ Pa. Reflectivity spectra of near normal incidence (~10°) were measured in the region of 3 to 20 eV with a typical resolution of 0.5 nm. The electric vector of the incident light was parallel to the *a*-axis (***E***//***a***) or *c*-axis (***E***//***c***) of the crystals. Since the cracking along the plane perpendicular to the *c*-axis occurs easily in $PbMoO_4$ crystals under rapid temperature change [24], the samples were cooled down slowly at a rate less than 2.5 K/min for measurements at 6 K.

XPS spectra were measured using an ESCA spectrometer (ULVAC-PHI 5600). The measurements were performed for a freshly cleaved sample surface. Monochromatized x-ray ($K_\alpha$: 1486.6 eV) from an Al anode was used for excitation. An electron flood gun was employed to compensate for the sample charging under x-ray irradiation. The overall resolution was about 0.5 eV under our experimental conditions. The base pressure in the sample chamber was less than $6.0 \times 10^{-8}$ Pa during the measurements.

**3 Results** The reflectivity spectra measured for samples of BARC and Furukawa agreed well with each other, except for slight differences in relative intensities of the structures. Figure 1 shows typical spectra of a Furukawa's sample at 6 K for the polarizations ***E***//***a*** and ***E***//***c*** in the 3–5 eV region. The absorption spectrum for ***E***//***a*** at 6 K is also shown. The steps below 3.4 eV in the reflectivity spectra are due to the reflection from the rear surface, since the sample is transparent in this region. The lowest exciton band around 3.6 eV clearly shows a doublet structure for ***E***//***a***. On the other hand, only a weak hump is seen in the 3.4–3.8 eV region for ***E***//***c***.

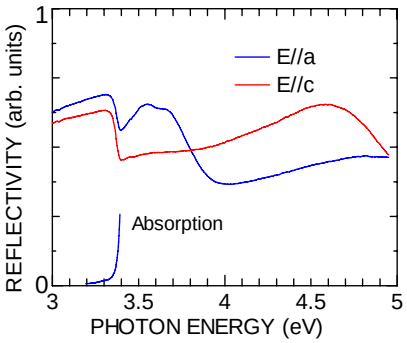


**Figure 1** (online colour at: www.pss-b.com) Reflectivity spectra for ***E***//***a*** and ***E***//***c*** at 6 K in the exciton band region. Absorption spectrum for ***E***//***a*** is also shown.

Because of the overlap of the reflection due to rear surface, it is difficult to obtain true spectra below fundamental absorption region. Therefore, the reflectivity *R* below the edge was calculated using the refractive index *n* and the relation $R = (n-1)^2/(n+1)^2$. The refractive indices of ordinary ray and extraordinary ray at room temperature [25] were used to calculate the reflectivity for ***E***//***a*** and ***E***//***c***, respectively. Each reflectivity spectrum measured above the absorption edge was connected to the calculated spectrum below the edge by multiplication with a constant factor.

The reflectivity spectra of $PbMoO_4$ at 6 K for ***E*//*a*** and ***E*//*c*** thus obtained are shown in Fig. 2 up to 20 eV. Remarkable dichroism is seen in the region below 6 eV. In the 6–10 eV region broad structures are observed for both polarizations. Main features above 4 eV reported in ref. [22] agree with those in Fig. 2.

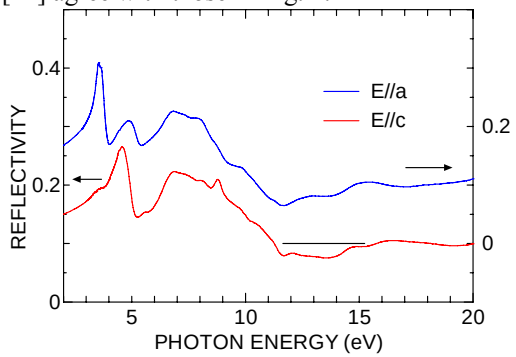


**Figure 2** (online colour at: www.pss-b.com) Reflectivity spectra of $PbMoO_4$ at 6 K for ***E*//*a*** and ***E*//*c***.

Optical constants were calculated from the spectra of Fig. 2 using a Kramers-Kronig analysis. Figures 3 and 4 show the real ($\varepsilon_1$) and imaginary ($\varepsilon_2$) parts of the dielectric functions, respectively. The $\varepsilon_2$ spectra below 6 eV are also shown in an expanded scale in Fig. 5. The lowest band 1 for ***E*//*a*** has two peaks $a_1$ at 3.58 eV and $a_2$ at 3.69 eV. On the other hand, the spectrum for ***E*//*c*** exhibits a weak plateau in this region. A broad peak 2 is observed at 4.7 eV for ***E*//*c***. The $\varepsilon_2$ spectra of $PbWO_4$ [18] are also shown in Fig. 5 for the sake of comparison.

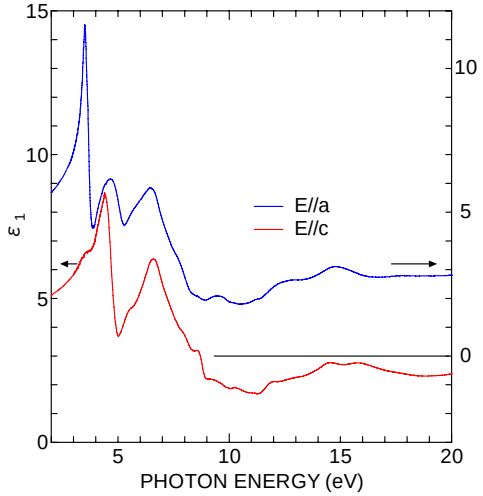


**Figure 3** (online colour at: www.pss-b.com) Real part of the dielectric function of $PbMoO_4$ for ***E*//*a*** and ***E*//*c*** at 6 K.

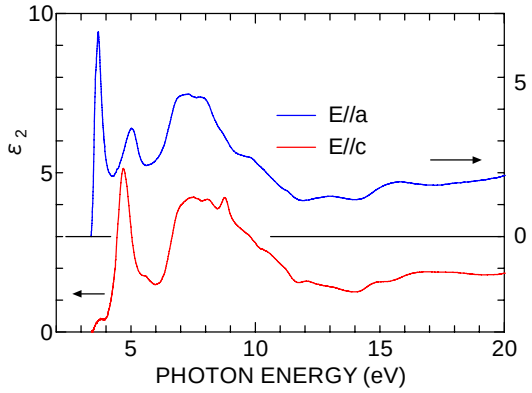


**Figure 4** (online colour at: www.pss-b.com) Imaginary part of the dielectric function of $PbMoO_4$ for ***E*//*a*** and ***E*//*c*** at 6 K.

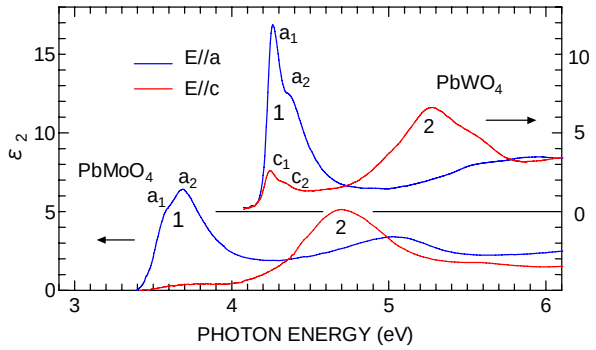


**Figure 5** (online colour at: www.pss-b.com) Imaginary part of the dielectric function of $PbMoO_4$ for ***E*//*a*** and ***E*//*c*** at 6 K in the region below 6 eV. The spectra of $PbWO_4$ [17] are also sown for comparison.

Common features are observed between the structures in $PbMoO_4$ and $PbWO_4$. The splitting of $a_1$ and $a_2$ in the lowest band 1 is 0.11 eV for $PbMoO_4$, and 0.12 eV for $PbWO_4$. The band 2 is observed at about 1 eV higher energy position for ***E*//*c*** in both materials. On the other hand, some differences are observed in Fig. 5. The intensity of the peak $a_1$ is stronger than that of $a_2$ in $PbWO_4$, and vice versa in $PbMoO_4$. In $PbWO_4$, peaks $c_1$ and $c_2$ are observed clearly, while no appreciable structure is seen on the weak plateau in the 3.4–4.0 eV region for ***E*//*c*** in $PbMoO_4$, although careful measurements were repeated using the samples of BARC and Furukawa. Since weak structures in reflectivity spectra are easily affected by the errors due to experimental noise and by the approximation in the Kramers-Kronig analysis, it is difficult to conclude whether any excitonic peaks exist or not for ***E*//*c*** of $PbMoO_4$. However, it is certain that the intensity of exciton absorption in this region for ***E*//*c*** of $PbMoO_4$ is extremely weak compared to that of $PbWO_4$.

Figure 6 shows the XPS spectrum of $PbMoO_4$ measured at 300 K. The binding energy is given relative to the top of the valence band. The full base width of the valence band is about 6 eV. The valence band shows two compo-

nents. There is a difference in the valence-band XPS spectra between $PbMoO_4$ and $PbWO_4$. In Fig. 6, the peak height of the high-binding energy component at 4.2 eV is almost the same as that of the low-binding energy one at 2.3 eV. On the other hand, the high-binding energy component in $PbWO_4$ is considerably stronger than that of the low-binding energy one [12]. A weak peak is observed at 7.0 eV. The doublet structure around 18 eV is due to the spin-orbit split Pb 5d core state; $5d_{5/2}$ and $5d_{3/2}$. The O 2s state is considered to be superposed on the Pb $5d_{3/2}$ band at around 19 eV. The spectral shape around the doublet structure is almost the same as that of $PbWO_4$ [12].

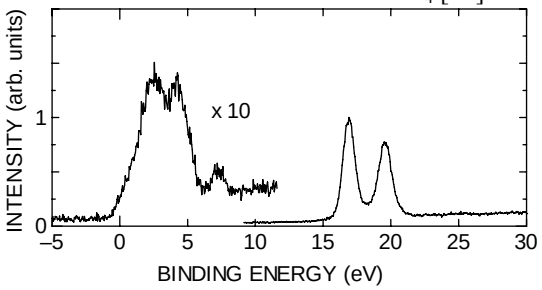


**Figure 6** XPS spectrum of $PbMoO_4$. The binding energy is given relative to the top of the valence band.

**4 Electronic structure of $PbMoO_4$ by the DV-*Xα* calculation** The electronic structure of $PbMoO_4$ and $PbWO_4$ has been calculated by the LAPW method [10]. The calculation suggests that the contribution of Pb states to the top of the valence band is small. This is incompatible with the experimental result on $PbWO_4$, where the exciton transition due to the intra-cationic excitation in Pb ions is obviously observed [18]. Recently the electronic structure of $PbMoO_4$ has been carried out by a density functional theory using CASTEP code [26]. The calculation shows the optical anisotropy of the fundamental absorption edge, that is, the absorption is stronger for ***E*//*a*** than for ***E*//*c***. This is consistent with the present experimental result in Fig. 5. In ref. [26], however, the partial density of states (PDOS) of the constituent atoms are not presented except for O 2p state. The information on the contibution of each atom is desired to discuss the origin of the structures in the optical spectra.

In the present study, the relativistic DV-*Xα* calculation was carried out for $PbMoO_4$. The details of the calculation method is described in ref. [27]. Three clusters $[Pb(MoO_4)_4]^{6-}$, $[Pb_9Mo_{10}O_{68}]^{58-}$, and $[Pb_4MoO_4]^{6+}$ were chosen to compare the calculated results with the experimental results in more convincing way. The band gap energies calculated from these clusters with taking the Madelung potential into account are 4.39 eV, 3.67 eV, and 5.04 eV, respectively. The band gap energy of $PbMoO_4$ has not been unambiguously determined. In the case of $PbWO_4$, it is estimated to be about 4.7 eV from the experiments of thermoluminescence [28] and photocurrent [29]. This reveals that the exciton binding energy for the peak $a_1$ in $PbWO_4$ is about 0.4 eV. If we assume the same value for $PbMoO_4$, the band gap energy is expected to be 4.0 eV. This value is in between the calculated band gap energies for clusters $[Pb(MoO_4)_4]^{6-}$ and $[Pb_9Mo_{10}O_{68}]^{58-}$. For reference, the calculated band gap energies by the LAPW method [10] and by the CASTEP code [26] are 2.59 eV and 4.5 eV, respectively.

In Fig. 7, we present the energy diagram and the PDOS of $PbMoO_4$ calculated for $[Pb(MoO_4)_4]^{6-}$ cluster for the sake of comparison with those of $PbWO_4$ in ref. [12], where the same cluster $[Pb(WO_4)_4]^{6-}$ was used. As shown in Fig. 7 the entire valence band is mainly built up of the O 2p state. The Pb 6s state hybridizes with the O 2p state at the top and the bottom of the valence band. In the lower part of the valence band the Mo 4d state hybridizes strongly with the O 2p state. The lower portion of the conduction band is dominated by the Mo 4d state which hybridizes with the Pb 6p and O 2p states. The partial contributions of the electronic states of Pb, O, and Mo atoms to the bottom of the conduction band are 8.2%, 26.4%, and 65.4%, respectively. The partial contributions of these atoms to the top of the valence band are 59.5%, 37.8%, and 2.7%, respectively. There are appreciable contributions of Pb state to the bottom of the conduction band and the top of the valence band, although the magnitudes are about 0.7 times as small as those in $PbWO_4$ (12.3% for conduction-band bottom and 84.7% for valence-band top) [12].

The Pb 5d and O 2p core states are situated at about –10 eV below the bottom of the valence band. The calculated binding energies of these core states are underestimated as compared to the XPS spectrum in Fig. 6. Similar underestimation is also found in the case of tungstates [12].

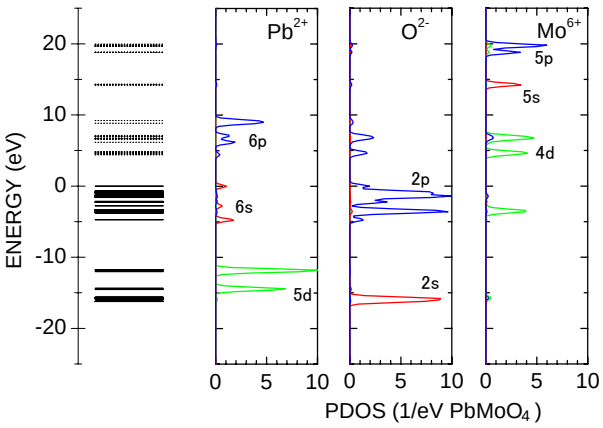


**Figure 7** (online colour at: www.pss-b.com) Energy diagram and partial density of states per molecule for $PbMoO_4$.

**5 Discussion** We first compare the XPS spectrum of $PbMoO_4$ in Fig. 6 with that of $PbWO_4$ in ref. [12]. It should be noted that the intensity of high-binding energy component in the valence band of $PbMoO_4$ is relatively weak compared to that of $PbWO_4$. Since the photoionization cross section of Mo 4d ($0.46\times10^{-2}$ Mb) is smaller than

that of W 5d ($0.65\times10^{-2}$ Mb) [30], this result reveals the existence of hybridization of the Mo 4d (W 5d) state with the O 2p state in the lower portion of the valence band in $PbMoO_4$ ($PbWO_4$). The above argument is in good agreement with the calculation result on PDOS of both materials. As for the weak band at 7.0 eV in Fig. 6, a similar band is also observed in $PbWO_4$. Two possible explanations for the origin of this band have been proposed [12]. One is that this band is attributed to the Pb 6s–O 2p bonding state which is found at −5.0 eV in Fig. 7. The other is that this band is due to the metallic Pb state produced at the sample surface during high-energy photon irradiation. The spectral shape of the doublet structure around 18 eV in Fig. 6 resembles that of $PbWO_4$ [12]. Such common feature is reasonable, because the doublet structure is due to the spin-orbit split Pb 5d states overlapping with the O 2p state in both materials.

Let us now consider the origin of band 1 and band 2 in $PbMoO_4$ in Fig. 5. In the previous paper [18], we proposed a model based on an intra-cationic Pb 6s → 6p transition in order to explain the dichroism of the exciton band in $PbWO_4$. There is a good similarity in the optical spectra between $PbMoO_4$ and $PbWO_4$, as shown in Fig. 5; i.e., the lowest band 1 shows doublet structure for $\boldsymbol{E}//\boldsymbol{a}$ and the band 2 is observed for $\boldsymbol{E}//\boldsymbol{c}$. Such a similarity suggests that the exciton transition in $PbMoO_4$ is also explained by the same model, although the calculated contributions of Pb state to the uppermost valence band and the lowest conduction band are not so large compared to those in $PbWO_4$. Here we describe the model in brief. In the scheelite structure, a $Pb^{2+}$ ion is at the site of $S_4$ symmetry surrounded by eight $O^{2-}$ ions. The Pb 6p state splits into the $\Gamma_{3,4}$ level and the $\Gamma_2$ level due to the uniaxial crystal-field along the *c*-axis [31]. The electric dipole transitions from the ground state $\Gamma_1$ of Pb 6s state to the former and the latter levels are allowed for the polarizations $\boldsymbol{E}//\boldsymbol{a}$ and $\boldsymbol{E}//\boldsymbol{c}$, respectively. The band 1 observed for $\boldsymbol{E}//\boldsymbol{a}$ and the band 2 for $\boldsymbol{E}//\boldsymbol{c}$ in Fig. 5 are ascribed to the transitions from the top of the valence band of the $\Gamma_1$ level to the $\Gamma_{3,4}$ level and the $\Gamma_2$ level, respectively. The splitting of the peaks $a_1$ and $a_2$ of the band 1 is attributed to the spin-orbit splitting of the Pb 6p state [18].

From the separation of band 1 and band 2, the crystal field splitting of the $\Gamma_{3,4}$ and $\Gamma_2$ states is estimated to be 1.0 eV for $PbMoO_4$, which is in good agreement with 0.9 eV for $PbWO_4$ [18]. Since the nearest neighbor Pb–O distance is nearly identical in $PbMoO_4$ (2.61 A) and $PbWO_4$ (2.59 A), it is reasonable that the crystal field splitting is not sensitive to the substitution of Mo for W. The spin-orbit coupling constant is evaluated to be almost the same (0.10 eV) in $PbMoO_4$ and $PbWO_4$ from the splitting of the peaks $a_1$ and $a_2$. The magnitude of the spin-orbit coupling is significantly reduced from that of a free $Pb^{2+}$ ion (1.63 eV) [32]. This reduction is due to the strong hybridization of Mo 4d (W 5d) state with the Pb 6p state in the conduction band as suggested from the DV-*Xα* calculations.

As far as the separation of band 1 and band 2 and the splitting of $a_1$ and $a_2$ are concerned, the above model explains the observed optical spectra well. However, there remain two questions to be considered. The intensity of peak $a_1$ is stronger than that of $a_2$ in $PbWO_4$, while the intensity ratio is inverted in $PbMoO_4$. Furthermore, in the spectrum of $PbWO_4$, small but distinct peaks $c_1$ and $c_2$ are observed for $\boldsymbol{E}//\boldsymbol{c}$, while such structures are not obvious in $PbMoO_4$.

Here, we point out that the electron-hole exchange interaction may play an important role in the exciton transitions in tungstates and molybdates. It is well known that alkali halides exhibit a pronounced doublet structure (halogen doublet) at the fundamental absorption edge due to exciton transition from the valence band of halogen p state to the conduction band of alkali s state [33, 34]. The doublet structure is attributed to the spin-orbit splitting of the halogen p state. Onodera and Toyozawa [35] have shown theoretically that the intensity ratio of the halogen doublet sensitively depends on the electron-hole exchange energy, while the doublet splitting is not so sensitive. As mentioned before, the contributions of Pb state to the top of the valence band and the bottom of the conduction band in $PbMoO_4$ are about 0.7 times as small as those in $PbWO_4$. This suggests that the wave functions of the electron and hole composing an exciton are localized to a lesser extent on a Pb ion in $PbMoO_4$, resulting in smaller overlap of the wave functions of electron and hole. The magnitude of the exchange interaction in $PbMoO_4$ is thus expected to be considerably small compared to that in $PbWO_4$, since the exchange interaction largely depends upon the overlap. If this speculation is correct, the difference in magnitude of the electron-hole exchange energy is responsible for the reversal of the intensity ratio of the structures $a_1$ and $a_2$ between $PbMoO_4$ and $PbWO_4$.

The exciton transition for $\boldsymbol{E}//\boldsymbol{c}$ in $PbMoO_4$ is very weak compared to that in $PbWO_4$ as shown in Fig. 5. The optical transition from the $\Gamma_1$ level to the $\Gamma_{3,4}$ level is forbidden for $\boldsymbol{E}//\boldsymbol{c}$ under the crystal field along the *c*-axis, as mentioned before. When the spin-orbit interaction and the electron-hole exchange interaction are taken into account, the transition becomes partially allowed for $\boldsymbol{E}//\boldsymbol{c}$. It is therefore supposed that the intensity of the transition for $\boldsymbol{E}//\boldsymbol{c}$ depends on the magnitudes of the crystal-field potential, spin-orbit coupling constant, and electron-hole exchange energy. In order to explain the transition intensity of each structure for $\boldsymbol{E}//\boldsymbol{a}$ and $\boldsymbol{E}//\boldsymbol{c}$ of $PbMoO_4$ and $PbWO_4$, a quantitative analysis using the parameters of these interactions would be required, but it is beyond the scope of this paper.

In the higher energy region, optical transitions from the O 2p state to the Mo 4d state are expected to occur, since the valence band is dominated by the O 2p state and the conduction band mainly consists of the Mo 4d state as shown in Fig. 7. In Fig. 4, a peak is observed at 5.1 eV for $\boldsymbol{E}//\boldsymbol{a}$, and broad structures are observed in the 7–9 eV region for both polarizations. These structures are likely assigned to the transitions from the O 2p state to the Mo 4d

state. Similar absorption bands due to the O 2p → Mo 4d transitions are also observed in $CaMoO_4$ crystals [19].

It is worth noting the relaxation processes of free excitons into self-trapped states in $PbMoO_4$ and $PbWO_4$ crystals. In both materials, the excitons are created on $Pb^{2+}$ ions, while the intrinsic luminescence arises from the radiative recombination of self-trapped excitons located on $(MoO_4)^{2-}$ or $(WO_4)^{2-}$ ions [5–9]. From these observations, we suppose that optically created excitons in $PbMoO_4$ and $PbWO_4$ move freely though the crystal during their lifetimes, and then self-trap on $(MoO_4)^{2-}$ or $(WO_4)^{2-}$ ions by inducing the Jahn-Teller distortion of the tetrahedral oxyanion molecules [9]. This situation is in clear contrast with that in other molybdates and tungstates, such as $CaMoO_4$ and $CaWO_4$ [19], where an electron-hole pair is created on a $(MoO_4)^{2-}$ or $(WO_4)^{2-}$ ion site, and subsequently self-traps on its site from which the intrinsic luminescence is emitted.

**6 Summary** We measured polarized reflectivity spectra of $PbMoO_4$ crystals. The optical constants for *a*- and *c*-axes were obtained. It was clarified that the exciton band has a doublet structure with remarkable dichroism. The measurement of XPS spectrum and the calculation of electronic structure by DV-*Xα* method were also carried out. The present results of $PbMoO_4$ were compared with the previous results of $PbWO_4$. The difference in valence-band XPS spectrum was ascribed to different magnitude of hybridization of Mo 4d or W 5d state to the O 2p state. From the energy band calculation and the similarity of optical spectra of $PbMoO_4$ and $PbWO_4$, it was pointed out that the exciton transition is explained by the cationic excitation model. The importance of the electron-hole exchange interaction in the exciton transition was suggested from the comparison of the fine structures in the exciton bands in $PbMoO_4$ and $PbWO_4$.

**Acknowledgements** The authors are indebted to Mr. T. Aoki and to Mr. R. Ogino for their assistance in optical measurement and in theoretical calculation, respectively. This work was supported by the Joint Studies Program of the Institute for Molecular Science.

## References

[1] M. Kobayashi, M. Ishii, Y. Usuki, and H. Yahagi, Nucl. Instrum. Methods Phys. Res. A **333**, 429 (1993).
[2] P. Lecoq, I. Dafinei, E. Auffray, M. Schneegans, M. V. Korzhik, O. V. Missevitch, V. B. Pavlenko, A. A. Fedorov, A. N. Annenkov, V. L. Kostylev, and V. D. Ligun, Nucl. Instrum. Methods Phys. Res. A **365**, 291 (1995).
[3] W. W. Moses, in: Proceedings of the Fifth International Conference on Inorganic Scintillators and Their Applications, Moscow, Russia, 1999 (Moscow State University, Moscow, 2000), p. 11.
[4] M. Kobayashi, Y. Usuki, M. Ishii, M. Itoh, and M. Nikl, Nucl. Instrum. Methods Phys. Res. A **540**, 381 (2005).
[5] W. van Loo, Phys. Status Solidi A **28**, 227 (1975).
[6] J. A. Groenink and G. Blasse, J. Solid State Chem. **32**, 9 (1980).
[7] M. Nikl, Phys. Status Solidi A **178**, 595 (2000).
[8] A. Krasnikov, M. Nikl, and S. Zazubovich, Phys. Status Solidi B **243**, 1727 (2006).
[9] M. Itoh and T. Sakurai, Phys. Rev. B **73**, 235106 (2006).
[10] Y. Zhang, N. A. W. Holzwarth, and R. T. Williams, Phys. Rev. B **57**, 12738 (1998).
[11] Y. Abraham, N. A. W. Holzwarth, and R. T. Williams, Phys. Rev. B **62**, 1733 (2000).
[12] M. Itoh, N. Fujita, and Y. Inabe, J. Phys. Soc. Jpn. **75**, 084705 (2006).
[13] R. W. G. Wyckoff, Crystal Structures, 2nd ed. (Wiley, New York, 1965), Vol. 3, Chap. VIII .
[14] M. Daturi, M. M. Borel, A. Leclaire, L. Savary, G. Costentin, J. C. Lavalley, and B. Raveau, J. Chim. Phys. Phys.-Chim. Biol. **93**, 2043 (1996).
[15] P. F. Schofield, K. S. Knight, S. A. T. Redfern, and G. Cressey, Acta Crystallogr., Sect. B: Struct. Sci. **B53**, 102 (1997).
[16] H. Kraus, V. B. Mikhailik, L. Vasylechko, D. Day, K. B. Hutton, J. Telfer, and Yu. Prots, Phys. Status Solidi A **204**, 730 (2007).
[17] M. Itoh and M. Fujita, Phys. Rev. B **62**, 12825 (2000).
[18] M. Fujita, M. Itoh, M. Horimoto, and H. Yokota, Phys. Rev. B **65**, 195105 (2002).
[19] M. Fujita, M. Itoh, S. Takagi, T. Shimizu, and N. Fujita, Phys. Status Solidi B **243**, 1898 (2006).
[20] M. Itoh, T. Katagiri, T. Aoki, and M. Fujita, Radiat. Meas. **42**, 545 (2007).
[21] M. Fujita, M. Itoh, T. Katagiri, D. Iri, M. Kitaura, and V. B. Mikhailik, Phys. Rev. B **77**, 155118 (2008).
[22] D. A. Spassky, S. N. Ivanov, V. N. Kolobanov, V. V. Mikhailin, V. N. Zemoskov, B. I. Zadneprovski, and L. I. Potkin, Radiat. Meas. **38**, 607 (2004)
[23] M. Tyagi, Sangeeta, D. G. Desai, and S. C. Sabharwal, J. Lumin. **128**, 22 (2008).
[24] Sangeeta, D. G. Desai, A. K. Singh, M. Tyagi, and S. C. Sabharwal, J. Crystal Growth **296**, 81 (2006).
[25] G. F. Bakhshieva and A. M. Morozov, Sov. J. Opt. Thechnol. **44**, 542 (1977).
[26] J. Chen, T. Liu, D. Cao, and G. Zhao, Phys. Status Solidi B **245**, 1152 (2008).
[27] H. Adachi, M. Tsukada, and C. Satoko, J. Phys. Soc. Jpn. 45, 875 (1978).
[28] V. Mürk, M. Nikl, E. Mihoková, and K. Nitsch, J. Phys.: Condens. Matter **9**, 249 (1997).
[29] C. Itoh and S. Kigoshi, Phys. Status Solidi A **203**, 3774 (2006).
[30] J. J. Yeh and I. Lindau, At. Data Nucl. Data Tables **32** 1 (1985).
[31] In ref. [18] we used the Bethe notation, while in refs. [19, 21] we used the Muliken notation. The representations $\Gamma_1$, $\Gamma_2$ and $\Gamma_{3,4}$ in the former correspond to *a*, *b* and *e* in the latter, respectively.
[32] W. C. Martin, J. Sugar, and J. L. Tech, Phys. Rev. A **6** 2022 (1972).

[33] J. E. Eby, K. J. Teegarden, and D. B. Dutton, Phys. Rev. **116**, 1099 (1959).
[34] T. Miyata, J. Phys. Soc. Jpn. **31**, 529 (1971).
[35] Y. Onodera and Y. Toyozawa, J. Phys. Soc. Jpn. **22**, 833 (1967).